AEROSPACE REPORT NO.
TR-2010(8550)-4

Life Test of 76-Ah Nickel-Hydrogen Cell Designs after 14 Years of Storage

10 January 2010

Albert H. Zimmerman and Michael V. Quinzio
Electronics and Photonics Laboratory
Physical Sciences Laboratories

Prepared for:

Space and Missile Systems Center
Air Force Space Command
483 N. Aviation Blvd.
El Segundo, CA 90245-2808

Authorized by: Engineering and Technology Group

APPROVED FOR PUBLIC RELEASE;
DISTRIBUTION UNLIMITED

AEROSPACE
Assuring Space Mission Success

This report was submitted by The Aerospace Corporation, El Segundo, CA 90245-4691, under Contract No. FA8802-09-C-0001 with the Space and Missile Systems Center, 483 N. Aviation Blvd., El Segundo, CA 90245. It was reviewed and approved for The Aerospace Corporation by B. Jaduszliwer, Principal Director, Electronics and Photonics Laboratory; and D. C. Marvin, Principal Director, Research and Program Development Office. David E. Davis was the project officer for the Mission-Oriented Investigation and Experimentation (MOIE) program.

This report has been reviewed by the Public Affairs Office (PAS) and is releasable to the National Technical Information Service (NTIS). At NTIS, it will be available to the general public, including foreign nationals.

This technical report has been reviewed and is approved for publication. Publication of this report does not constitute Air Force approval of the report's findings or conclusions. It is published only for the exchange and stimulation of ideas.

Luis Rodriguez Jan. 29, 2010

* David E. Davis
SMC/EA

* Signing for Mr. Dave Davis

REPORT DOCUMENTATION PAGE

Form Approved
OMB No. 0704-0188

Public reporting burden for this collection of information is estimated to average 1 hour per response, including the time for reviewing instructions, searching existing data sources, gathering and maintaining the data needed, and completing and reviewing this collection of information. Send comments regarding this burden estimate or any other aspect of this collection of information, including suggestions for reducing this burden to Department of Defense, Washington Headquarters Services, Directorate for Information Operations and Reports (0704-0188), 1215 Jefferson Davis Highway, Suite 1204, Arlington, VA 22202-4302. Respondents should be aware that notwithstanding any other provision of law, no person shall be subject to any penalty for failing to comply with a collection of information if it does not display a currently valid OMB control number. **PLEASE DO NOT RETURN YOUR FORM TO THE ABOVE ADDRESS.**

1. REPORT DATE (*DD-MM-YYYY*)	2. REPORT TYPE	3. DATES COVERED *(From - To)*
10-01-2010		

4. TITLE AND SUBTITLE

Life Test of 76-Ah Nickel-Hydrogen Cell Designs after 14 Years of Storage

5a. CONTRACT NUMBER
FA8802-09-C-0001

5b. GRANT NUMBER

5c. PROGRAM ELEMENT NUMBER

6. AUTHOR(S)

Albert H. Zimmerman and Michael V. Quinzio

5d. PROJECT NUMBER

5e. TASK NUMBER

5f. WORK UNIT NUMBER

7. PERFORMING ORGANIZATION NAME(S) AND ADDRESS(ES)

The Aerospace Corporation
Physical Sciences Laboratories
El Segundo, CA 90245-4691

8. PERFORMING ORGANIZATION REPORT NUMBER

TR-2010(8550)-4

9. SPONSORING / MONITORING AGENCY NAME(S) AND ADDRESS(ES)

Space and Missile Systems Center
Air Force Space Command
483 N. Aviation Blvd.
El Segundo, CA 90245

10. SPONSOR/MONITOR'S ACRONYM(S)
SMC

11. SPONSOR/MONITOR'S REPORT NUMBER(S)

12. DISTRIBUTION/AVAILABILITY STATEMENT

Approved for public release; distribution unlimited.

13. SUPPLEMENTARY NOTES

20100310201

14. ABSTRACT

A matrix of twelve nickel-hydrogen cells were built in 1988 to develop and validate the ManTech nickel-hydrogen cell design that has subsequently been used in a wide range of space applications. This cell matrix included three design variations: precharge (hydrogen or nickel), electrolyte concentration (31% or 38%), and electrolyte amount (drained or drained plus 20 cc). In 2003, eight of these cells were put into a life test following 14 years of continuous discharged storage to evaluate the effects of long-term storage on the cycle life of each design variant. Two of the cells have failed, and several of the other cells have shown evidence of degradation to date after more than six years of cycling. All the cells that have failed or degraded are those with the higher electrolyte concentration, which is a design variant that was abandoned in 1989 because of its lower expected life capability. The six non-failed cells, including two cells representative of the final ManTech design that has been used for decades, continue to cycle in this life test.

15. SUBJECT TERMS

Battery, Nickel hydrogen, Short circuit, Capacity loss, Life test, Precharge, Electrolyte concentration

16. SECURITY CLASSIFICATION OF:			17. LIMITATION OF ABSTRACT	18. NUMBER OF PAGES	19a. NAME OF RESPONSIBLE PERSON
					Albert Zimmerman
a. REPORT	b. ABSTRACT	c. THIS PAGE	Leave blank	19	19b. TELEPHONE NUMBER *(include area code)*
UNCLASSIFIED	UNCLASSIFIED	UNCLASSIFIED			(310)336-7415

Contents

Figures

Tables

1. Introduction

In 1988, twelve 76-Ah nickel-hydrogen cells were manufactured by EaglePicher to test and validate their ManTech nickel-hydrogen design. The results of the early testing on these cells were used as the basis for the ManTech cell design that has been widely used in space applications during the past 20 years. The twelve cells represent a matrix of three differing design combinations that use different precharge, different electrolyte concentration, and differing amounts of electrolyte. The design variants in these twelve cells are shown in Table 1. All cells contain two layers of Zircar separator in a back-to-back stack, and had a maximum expected operating pressure of about 1000 psi.

The precharge variations in Table 1 consist of either 1 atm of hydrogen precharge or a nickel electrode precharge of about 15% of nameplate cell capacity. The electrolyte concentrations consist of 38%, which was from the earlier Comsat cell design, or the lower 31%. The KOH backfill indicates the amount of electrolyte of the appropriate concentration that was added back to the cell after all free electrolyte had been drained.

Following initial testing of these cells for the purpose of selecting the best ManTech design,* which was designated as the RNH 76-11 design, eight of the cells were shipped to The Aerospace Corporation for test purposes. These eight cells were operated in several capacity and special charge retention tests in 1989, and then placed into continuous discharged storage at approximately 23°C until 2003. In October of 2003, a life test was begun on these cells to gather data to indicate how the ~14 years of

Table 1. Matrix of Design Variations for Test Cells

Cell S/N	Precharge	KOH Electrolyte Concentration	KOH Backfill	Cell # In This Test
1	hydrogen	38%	none	6
2	hydrogen	31%	none	5
3	hydrogen	38%	20 cm^3	**
4	hydrogen	31%	20 cm^3	8
5	hydrogen	38%	none	2 (failed)
6	hydrogen	31%	none	**
7	nickel	38%	20 cm^3	**
8	nickel	31%	20 cm^3	**
9	nickel	38%	none	1 (failed)
10	nickel	31%	none	4
11	nickel	38%	20 cm^3	7
12	nickel	31%	20 cm^3	3

**Cell not available: consumed in initial design selection testing

* The optimum ManTech design selected had the nickel precharge, 31% KOH electrolyte, and no backfill. The nickel precharge was selected for improved cell capacity stability during storage, the 31% KOH was selected for improved life relative to higher concentrations, and there was concern that the KOH backfill could accentuate popping damage issues.

storage had affected the life capability of each of the cell designs. The last column in Table I indicates the position number for each cell included in this eight-cell test.

2. Life Test Description

This life test repeatedly runs the cells through a sequence of 45 cycles, with one cycle per day. The durations of the charge and discharge periods during each day in the sequence, as well as the discharge currents and depth of discharge (DOD) are provided in Table 2. The peak depth of discharge, which occurs on day 23 of the sequence, is 56.31%. For each cycle, recharge is done at 6.5 A until a 1.1 recharge ratio is reached, and then the current is reduced to 0.7 A for the remainder of the charge time.

After each 45-day cycling sequence is completed, each cell is discharged at C/2 (38 A) to 0.7 V, followed by discharge at C/20 (3.8 A) to 0.6 V to perform a reconditioning. Recharge is then done at C/10 (7.6 A) for 16 h, after which the cells are again discharged completely at C/2 and then C/20 to measure their reconditioned performance. A full recharge at C/10 for 16 h is then done again before starting the next 45-day cycling sequence. The cell temperatures are maintained at roughly +5°C during the 0.7-A charge periods of the cycling.

Table 2. Charge and Discharge Parameters for 45-Day Cycling Sequence

Day	Discharge (s)	Discharge (A)	Charge Time (s)	DOD (%)	Day	Discharge (s)	Discharge (A)	Charge time (s)	DOD (%)
1	1560	34.57	84840	19.71	24	4320	35.63	82080	56.25
2	2040	34.85	84360	25.98	25	4260	35.59	82140	55.42
3	2280	35.01	84120	29.17	26	4260	35.57	82140	55.39
4	2580	35.20	83820	33.19	27	4200	35.53	82200	54.55
5	2760	35.25	83640	35.56	28	4200	35.53	82200	54.54
6	3000	35.71	83400	39.16	29	4140	35.50	82260	53.72
7	3120	35.50	83280	40.48	30	4080	35.52	82320	52.97
8	3300	35.51	83100	42.83	31	4020	35.49	82380	52.15
9	3420	35.47	82980	44.33	32	3960	35.46	82440	51.33
10	3540	35.51	82860	45.95	33	3840	35.38	82560	49.66
11	3660	35.55	82740	47.55	34	3780	35.40	82620	48.90
12	3780	35.60	82620	49.18	35	3660	35.34	82740	47.28
13	3840	35.57	82560	49.92	36	3540	35.31	82860	45.68
14	3960	35.61	82440	51.54	37	3420	35.23	82980	44.04
15	4020	35.61	82380	52.33	38	3300	35.04	83100	42.26
16	4080	35.61	82320	53.11	39	3120	35.11	83280	40.04
17	4140	35.65	82260	53.94	40	3000	35.09	83400	38.47
18	4200	35.66	82200	54.74	41	2760	34.99	83640	35.29
19	4200	35.66	82200	54.74	42	2580	34.92	83820	32.93
20	4260	35.64	82140	55.49	43	2280	34.80	84120	29.00
21	4260	35.61	82140	55.45	44	2040	34.74	84360	25.90
22	4320	35.65	82080	56.29	45	1560	34.49	84840	19.67
23	4320	35.66	82080	56.31					

The entire sequence described above lasts about 47 days, thus enabling 7.75 sequences to be completed per year, for a nominal total of 365 cycles per year, assuming no test down time. Over the past 6 years, the down time for this test has averaged 5.38% of the elapsed calendar time. The down time has included test interruptions resulting from equipment failures or maintenance, as well as evaluation and reconfiguration after two cell failures. Failure of a cell in this test is defined by the inability for that cell to maintain 1.0 V at the end of discharge during the cycling sequence.

3. Cell Performance during the Life Test

This life test has completed 44 of the 45-day cycling sequences, amounting to 2020 total cycles over the approximately 6 years that it has been operating. The minimum voltage during each cycle (excluding the reconditioning and capacity check cycles after each sequence) are shown in Figure 1. As indicated in Figure 1, there have been several periods during the test where programming errors resulted in a few abbreviated or extended cycling sequences. The voltage of cell 5 appeared to be affected by a series resistance arising from the terminal connections that was estimated to be 4.43 mΩ. This has been constant at all times throughout this test for cell 5. The end of discharge voltage for cell 5 in Figure 1 has been corrected for this added resistance.

Inspection of Figure 1 shows that cell 2 developed some performance problems after about 700 cycles. This cell was declared as failed and removed from the test after 742 cycles, with the failure being caused by intermittent short circuit. Within the first 500 to 1000 cycles, cell 6 also developed a low end-of-discharge voltage from elevated internal impedance, although to date, cell 6 has not failed. After cycle 2020, cell 1 failed due to an internal short circuit, and was also removed from the test. Figure 1 shows cell 1 discharge voltage dropping for 400–500 cycles prior to its failure.

Figure 2 shows the peak recharge voltages during the cycling, which typically occurs at the end of the 6.5 A recharge when the 1.10 recharge ratio has been reached. All cells have remained in the range of about 1.48 to 1.53 V during the test. Elevated peak recharge voltages are seen just prior to the

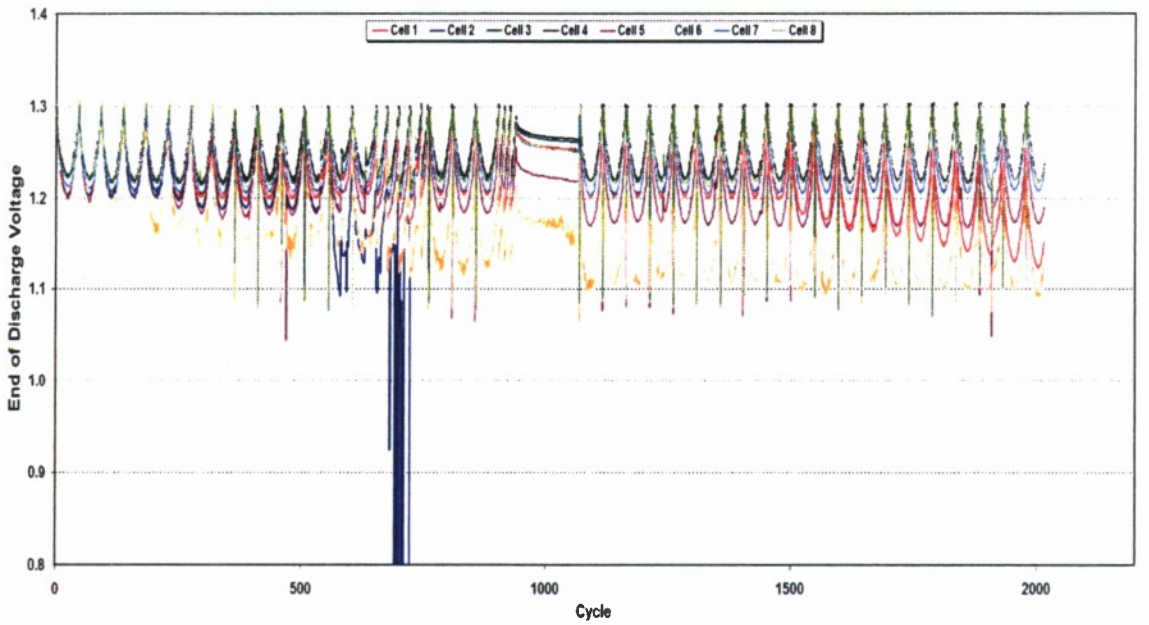

Figure 1. End of discharge voltage for each cell during cycling sequences completed.

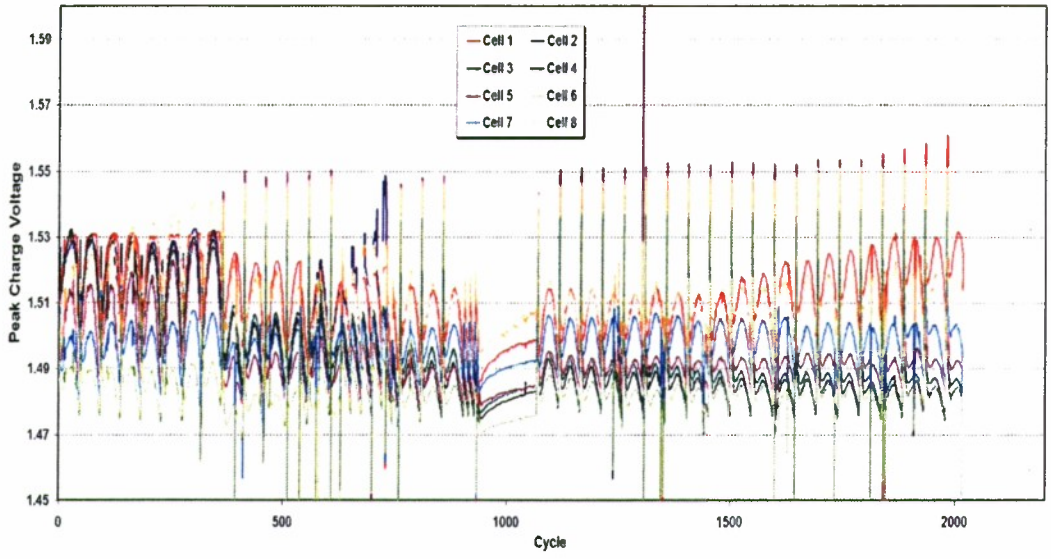

Figure 2. Peak recharge voltage for each cell during cycling sequences completed.

failure of cell 2 near 700 cycles, and then again for cell 1 near cycle 2000. The voltage spikes that periodically occur up to about 1.55 V are caused by the capacity check recharge done between each 45-day cycling sequence.

The test temperatures are shown in Figure 3. The significant temperature spikes occasionally seen above 9°C or below 3°C correspond to test problems that upset the chiller thermal control. Such events included power interruptions, bad data readings, and chiller malfunctions. The test temperature has been controlled such that the end-of-charge temperature was held at about 5°C. Discharge heating has resulted in a 2–3°C warming of cells at the end of discharge relative to end of charge.

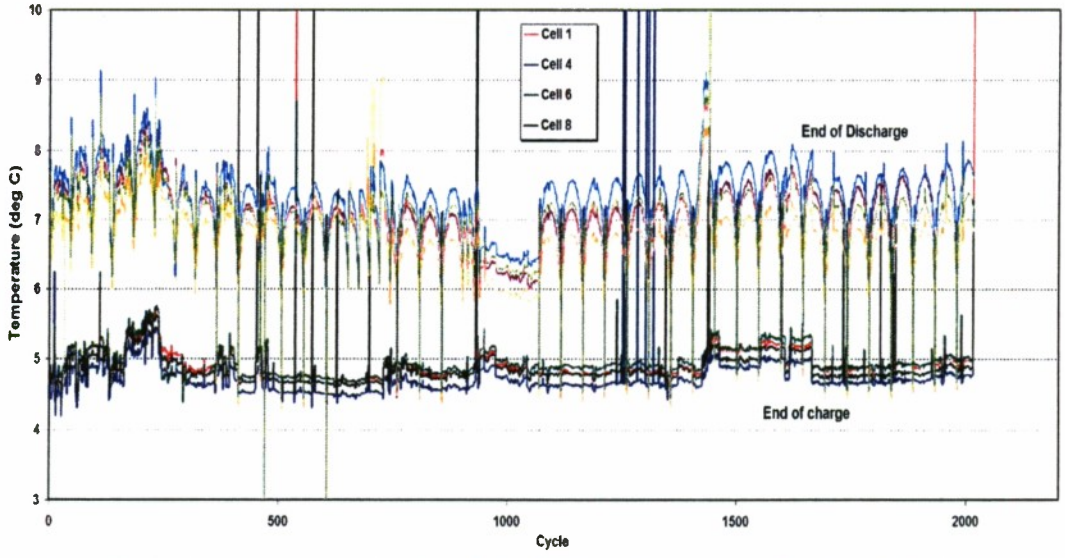

Figure 3. End of discharge and end of recharge temperatures for instrumented cells during cycling sequences completed. The test is being controlled to about a 5°C end of charge temperature.

After each 45-day cycling sequence, a capacity discharge is performed from the state of charge that the cells had at the end of the sequence, followed by a second capacity discharge after reconditioning. The cell capacities measured by these capacity checks after each sequence are plotted in Figure 4. The saw-tooth appearance of Figure 4 results from the first capacity measurement, which is directly from the cycling state of charge, always being lower than the second capacity, which is following reconditioning and a full recharge. The lower reconditioned capacity for the first 400 cycles results from the cells only being charged for 12 h following reconditioning, vs. 16 h later in the test. The capacities of all these cells have been relatively stable, with the notable exception of cell 1, which dropped about 15 Ah during the 500 cycles prior to its failure after cycle 2020. Cell 2 showed no significant capacity drop prior to its failure around cycle 700. The main reason for the anomalously low capacity for cell 5 is the extra resistance in the cell circuit, which is believed to be a test artifact since it has not varied with time, cell state of charge, or any other cell-related variable.

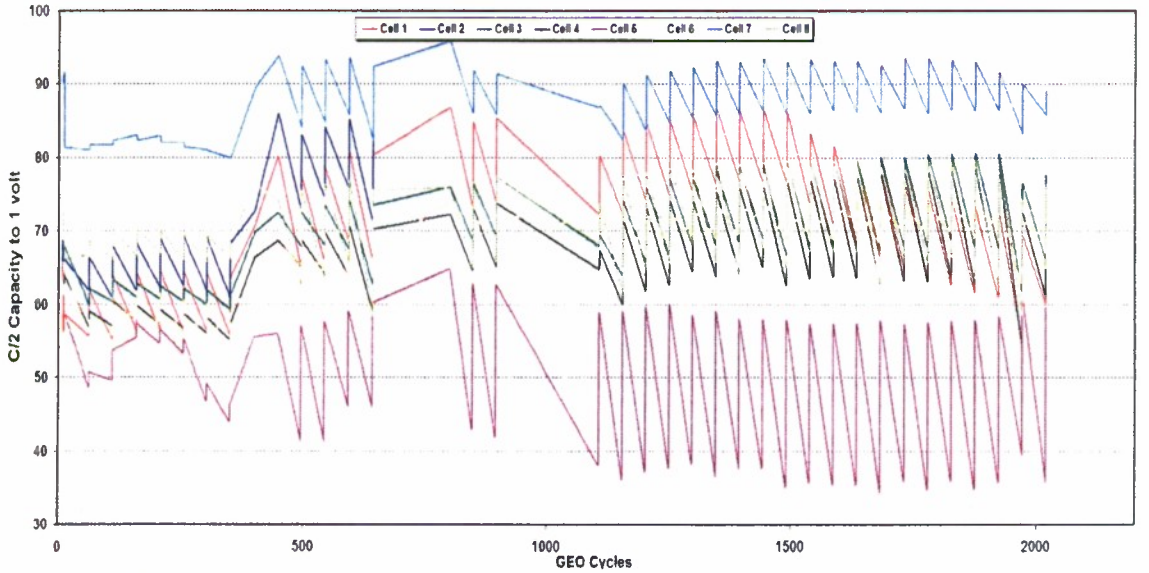

Figure 4. Capacity measurements after each cycling sequence. The lower one is directly from cycling, and the higher one is after reconditioning.

4. Cell Voltage Behavior

The charge and discharge voltage profiles and how they change during the testing can reveal much about what is occurring in a cell as it degrades. Figures 5 and 6 show the beginning of life discharge and recharge voltages for the cells. Figure 5 shows that the discharge voltage plateaus were similar for all the cells, except cell 5, which had an anomalous resistance in the cell connection wiring. However, all the cells except cell 7 displayed significant capacity loss relative to 76 Ah. These capacity losses range from less than 5% for cell 8 to about 25% for cells 5 and 6. It is believed that these capacity losses resulted from the 14 years of storage (over 15 years from cell activation). The cells with the greater amount of capacity losses tended to be the ones with hydrogen precharge, which is likely to be a contributing factor. It is not clear why cell 7 maintained much better capacity than all the other cells.

The recharge voltage profiles in Figure 6 clearly show that three of the cells had a hydrogen precharge at BOL (cells 5, 6, and 8), while the other cells had nickel precharge. This is recognized by the sharply increased voltage at the start of recharge, which is caused by a fully depleted nickel electrode. It is not clear why cell 2, which should have contained hydrogen precharge according to the test cell matrix of Table 1, showed nickel precharge here. This observation suggests there are factors that can affect the precharge settings enough to completely lose one atm of hydrogen precharge (one atm corresponds to only about 1.5% hydrogen precharge in this cell design).

The recharge profiles in Figure 6 also indicate which cells had the higher electrolyte concentration. The higher concentration stabilizes the formation of γ-NiOOH during overcharge, thus causing the charge voltage to peak, and then continue rising significantly as γ-NiOOH continues to be generated.

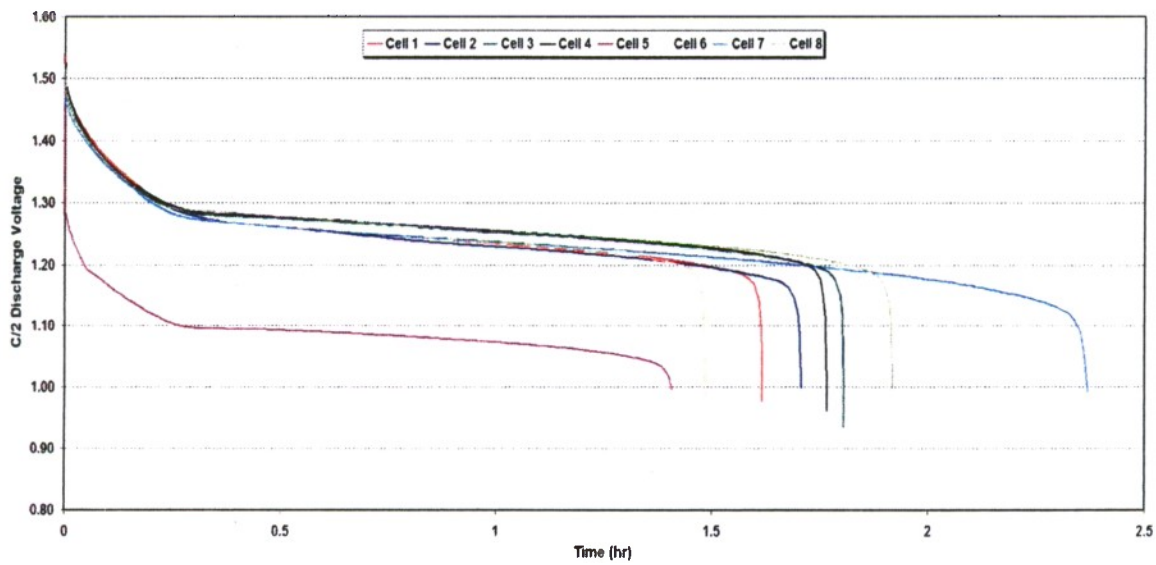

Figure 5. Discharge voltage profiles at beginning of life with a C/2 discharge rate.

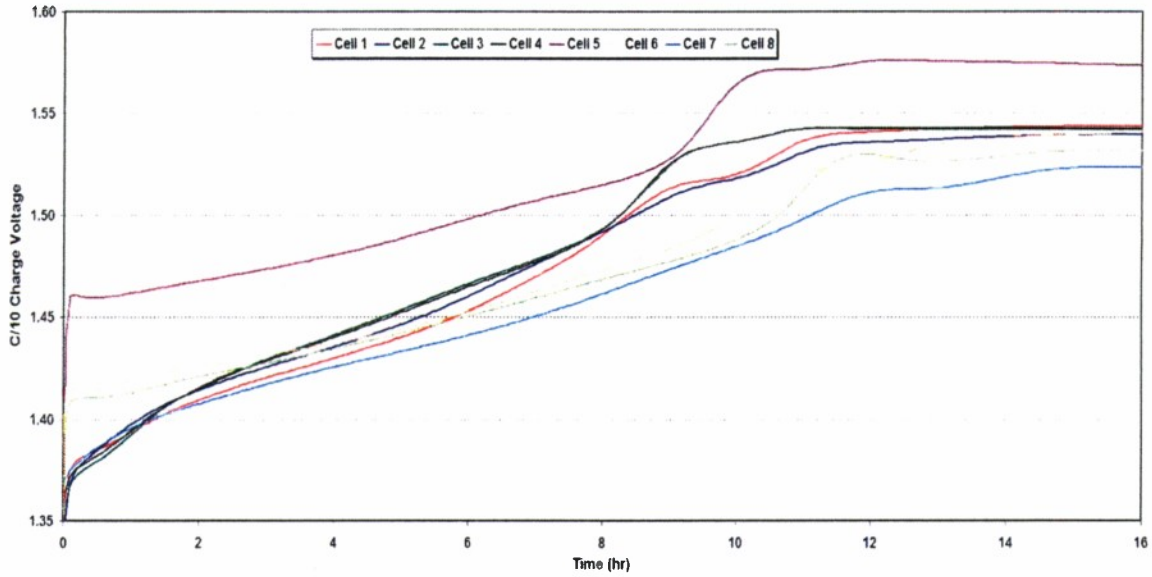

Figure 6. Recharge voltage profiles at beginning of life with a C/10 charge rate.

This is the profile seen for cells 1, 2, 6, and 7, which all contain the higher electrolyte concentration, as indicated in Table 1.

At the last post-reconditioning capacity check before cell 2 failed (cycle 643), the discharge and recharge voltage profiles are again plotted to determine how they had changed during the first 643 cycles. The results are shown in Figures 7 and 8. Figure 7 shows that significant discharge capacity was present in the form of a second plateau below 1 V for all cells. All the cells had significantly increased in capacity since the start of testing, with all except cells 2 and 5 attaining 76 Ah. Additionally, cells 2 and 6 had developed a decreased upper discharge voltage, which usually indicates resis-

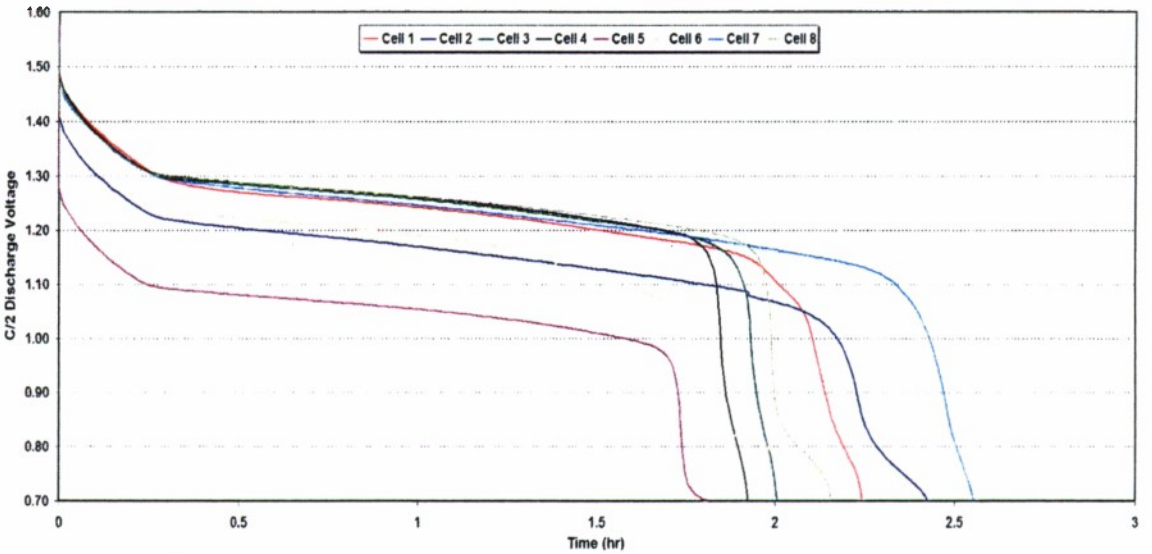

Figure 7. Discharge voltage profiles at cycle 643 with a C/2 discharge rate.

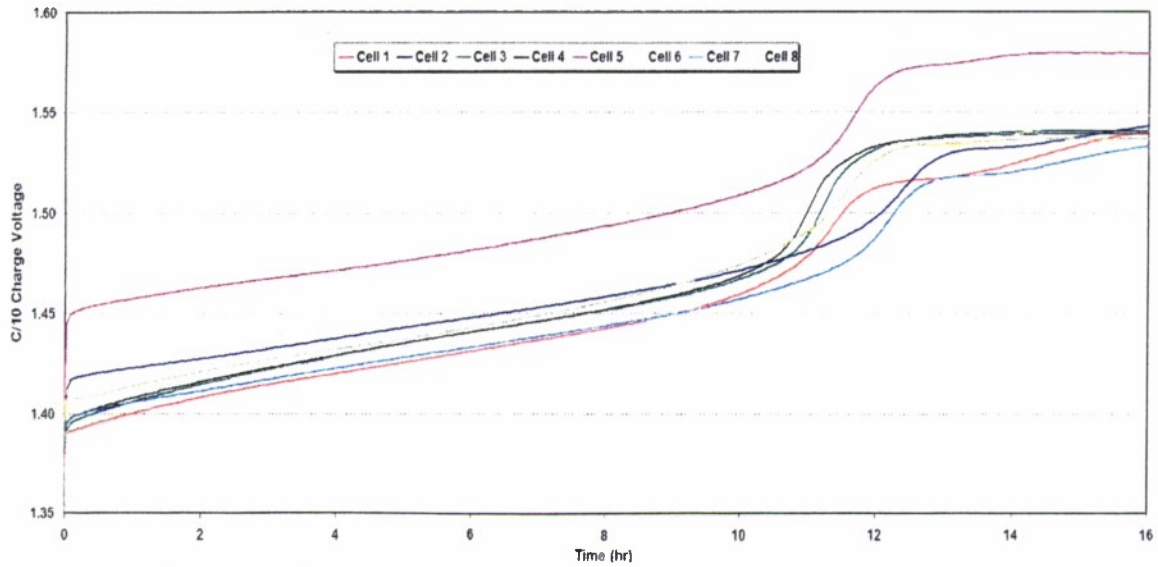

Figure 8. Recharge voltage profiles at cycle 643 with a C/10 charge rate.

tance from separator dry out. The drops in voltage for cells 2 and 6 at 1.5 to 2 h suggest that these cells may have intermittent shorting or impedance issues that could cause failure.

Figure 8 suggests that all the cells either had hydrogen precharge or were close to the hydrogen precharged condition after 643 cycles.

At the last capacity check before cell 1 failed (cycle 2020), the discharge and recharge voltage profiles are again plotted to determine how they had changed during the first 2020 cycles. The discharge results shown in Figure 9 do not include cell 2 because it had failed. The discharge measurements in

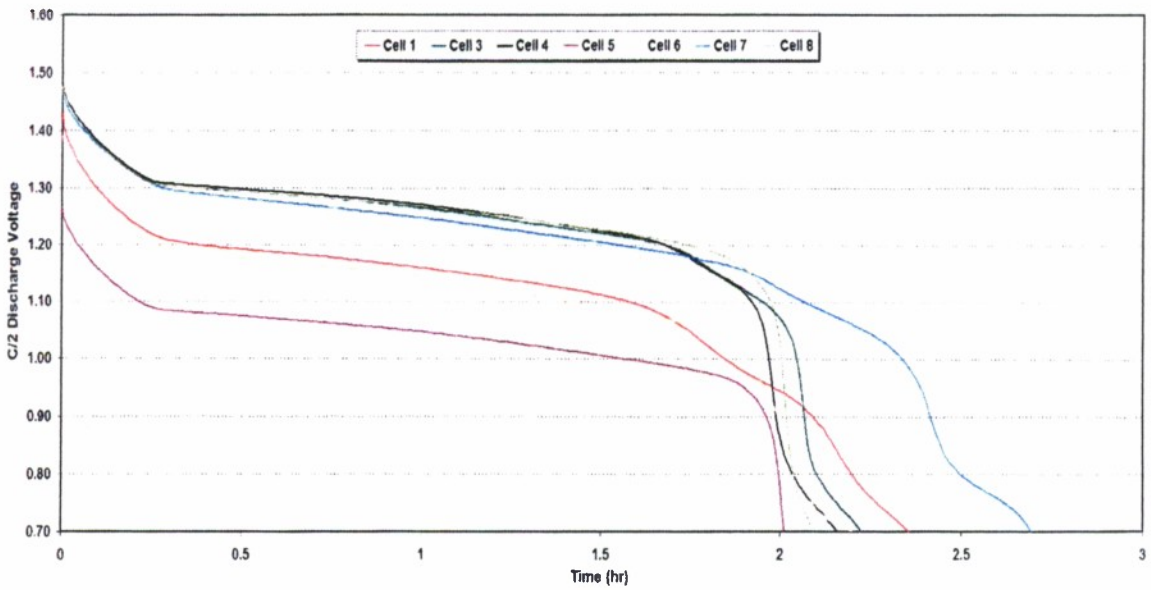

Figure 9. Discharge voltage profiles at cycle 2020 with a C/2 discharge rate.

Figure 9 show that the trend toward increased post-reconditioning capacity noted in Figure 7 after 643 cycles had continued, and all cells displayed at least 76 Ah of capacity. Cell 5 had 76 Ah above 1 V if the discharge voltage was adjusted for the 4.43 mΩ lead resistance that seems to be displacing the discharge voltage downward and the charge voltage upward. In addition, all cells appear to have a significant lower voltage plateau near 0.8 V that is not fully resolved in a discharge to 0.7 V.

Some interesting trends can be seen in the discharge data of Figure 9 that correlate with the design differences between the cells. First, the three remaining cells having high electrolyte concentration, cells 1, 6, and 7 (failed cell 2 was the fourth one with high concentration), all show evidence for a depressed discharge voltage plateau, although the depression is relatively small for cell 7. This signature typically is caused by separator dry out, which seems to be accentuated by the high electrolyte concentration. It is likely that the high electrolyte concentration causes accelerated swelling of the nickel electrodes, thus causing them to draw electrolyte out of the separator and raise its resistance.

A second interesting signature is seen in Figure 9 for all four of the cells that were manufactured with 15% nickel precharge, cells 1, 3, 4, and 7. Each of these cells displays a more rapidly declining segment of the upper discharge plateau at the end of the upper discharge plateau. This signature appears to be an emerging new discharge plateau that is roughly 50–100 mV lower than the normal discharge plateau. This plateau may correspond to discharge of γ-NiOOH, although it is significantly lower than the 1.20-V potential where γ-NiOOH normally undergoes discharge.[*] An alternative explanation is that this emerging lower plateau corresponds to a novel nickel electrode material, such as the Pt-Ni-Co complex described in Ref. 3, which has a discharge voltage about 100 mV below the normal discharge plateau. The emergence of this slightly low secondary discharge plateau clearly is associated with aging of the cells since it was barely perceptible in Figure 7 at cycle 643. A novel observation, however, is the observation of this slightly low secondary discharge plateau only in cells that were built with nickel precharge. This correlation suggests that the Pt-Ni-Co complex,[†] which is known to form in nickel precharged cells during long-term storage, may have a significant effect on cell performance after many years of operation following removal from storage. More importantly, this effect does not appear to be deleterious to performance since all the cells showing the slightly low secondary discharge plateau have very good capacity, particularly if capacity delivered at cell voltages between 1.1 and 1.2 V can be effectively used.

Figure 10 shows the charge voltage profiles for the cells after reconditioning at cycle 2020. Again, the discharge results shown in Figure 10 do not include cell 2 because it had failed. Figure 10 shows that all the cells that originally had nickel precharge have clearly developed a hydrogen precharge, as indicated by the sharp rise over 1.40 V and peaked voltage behavior at the start of the charge. The three remaining cells with higher concentration electrolyte (cells 1, 6, and 7) continue to display a pronounced secondary voltage rise after going into overcharge as γ-NiOOH is formed at the end of charge. Cycle 2020 was the last capacity check prior to the failure of cell 1. The recharge voltage for cell 1 only suggested that the capacity had degraded about 20%, and that the charge voltage had increased 10–20 mV, certainly not clear indications of imminent failure.

---

[*] Albert H. Zimmerman, *Nickel Hydrogen Batteries: Principles and Practice*, The Aerospace Press, El Segundo, CA, 2009, p. 113.

[†] Ibid. p. 131.

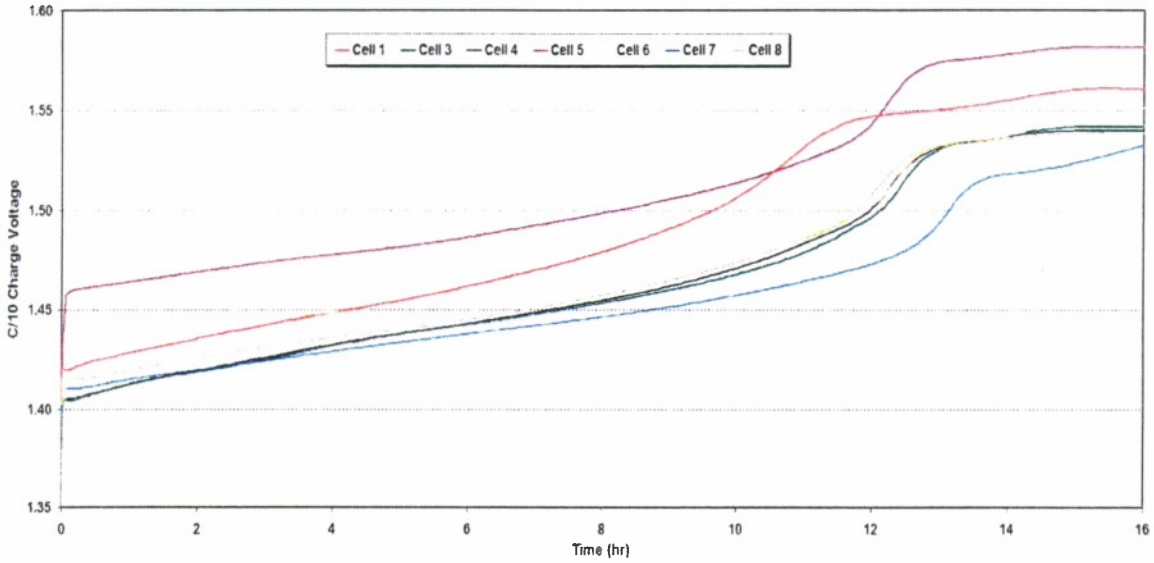

Figure 10. Recharge voltage profiles at cycle 2020 with a C/10 charge rate

5. Cell 2 Failure

As shown in Figure 1, cell 2 began displaying erratic voltages during discharge at about cycle 700. In Figure 7, the discharge curve at cycle 643 shows the beginnings of this erratic behavior as a small but sudden voltage drop almost 2 h into the capacity discharge. At cycle 768, the voltage of cell 2 had become so erratic that it could no longer continue cycling, and it was removed from the test. Figure 11 compares cycle 730, which was typical of the poorer performing cycles for this cell, to a cycle at the same depth of discharge early in life (cycle 56). Even near the end of its life, cell 2 occasionally gave cycles that were nearly normal in voltage performance.

After removal from the test station, cell 2 was subjected to three standard capacity cycles at 10°C. Both its voltage and capacity appeared normal during these cycles. The erratic voltages only seemed to appear after a number of cycles, becoming more erratic with time. The likely cause for the erratic voltages is variable soft shorting through the separation that gradually bleeds down cell capacity to below the threshold needed to support discharge above 1 V. These shorts seemed to come and go, but nearly always became worse during discharge when the nickel electrodes tend to undergo expansion. These observations suggest the failure is associated with nickel plate expansion, active material extrusion, and separator dry out, all which are likely to be accelerated by the higher electrolyte concentration and the absence of an electrolyte backfill in this cell. It is unclear whether the 14 years of storage with hydrogen precharge prior to testing contributed to this failure mode. It is also unclear why cell 2 failed so early in this test relative to the other cells. This could be an indication of degradation associated with the lengthy pre-test storage.

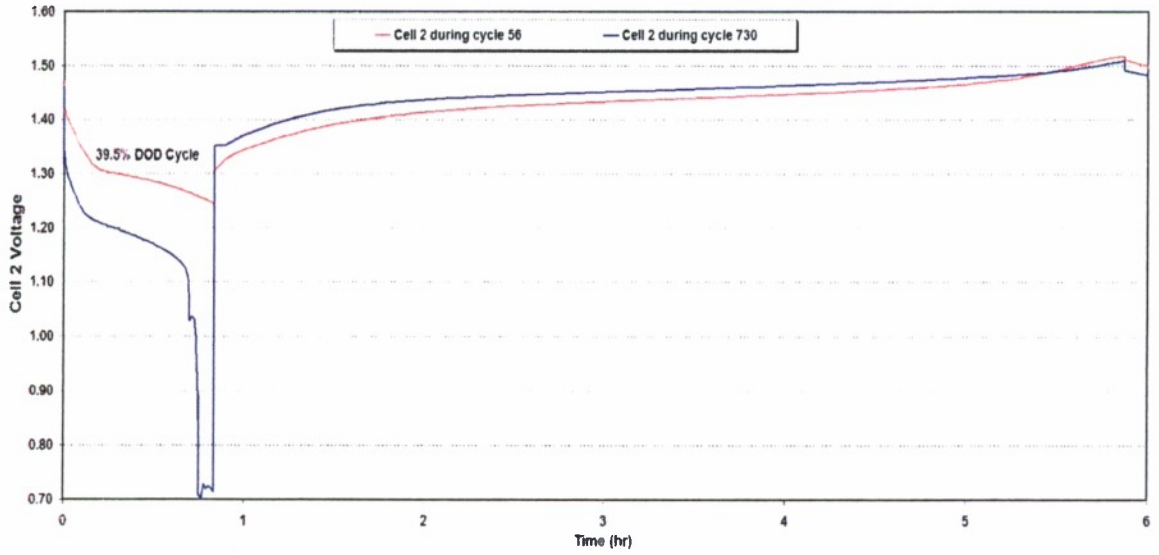

Figure 11. Erratic voltage signature displayed by cell 2 just prior to removal from the test.

6. Cell 1 Failure

As shown in Figure 1, cell 1 began gradually degrading in performance around cycle 1500. Figures 9 and 10 show the degradation had become quite significant by cycle 2020, amounting to about a 20% capacity loss. Figure 9 shows that an increasing cell resistance was associated with a drop in the discharge voltage plateau, indicative of anomalous resistance from separator dry out.

During cycle 2056, cell 1 developed an internal hard short that rapidly caused the cell to fail. The voltage and thermal signatures during cycle 2056, which accompanied this failure, are shown in Figure 12. The failure occurred precipitously during discharge (at 33.7% depth of discharge), and was characterized by a sudden drop in cell voltage to just above 1.00 V. At this point, the cell temperature began to rapidly increase. Discharge continued for about 4 min, whereupon the cells were open circuited because cell 1 temperature had increased to the maximum allowed limit of 15°C. Over the next 0.5 to 1.0 h, the cell voltage rose to just over 1.0 V for about 40 min and then began to drop toward 0 V. The cell temperature continued rising, and reached a maximum of nearly 70°C about 30 min after initiation of the short circuit. The voltage of the cell ultimately fell to zero, indicating that an internal hard short had developed in this cell.

Prior to disassembling cell 1 to determine the root cause for the failure, the hydrogen gas pressure in this cell was measured by puncturing the cell case and collecting the gas in an evacuated chamber. Using this method, the gas pressure within this shorted cell was 141.6 psia. This pressure indicates a significant pressure growth in this cell during the 6 years of cycling that it had experienced. It is very likely that some of this pressure growth could have occurred during the lengthy storage prior to starting this test.

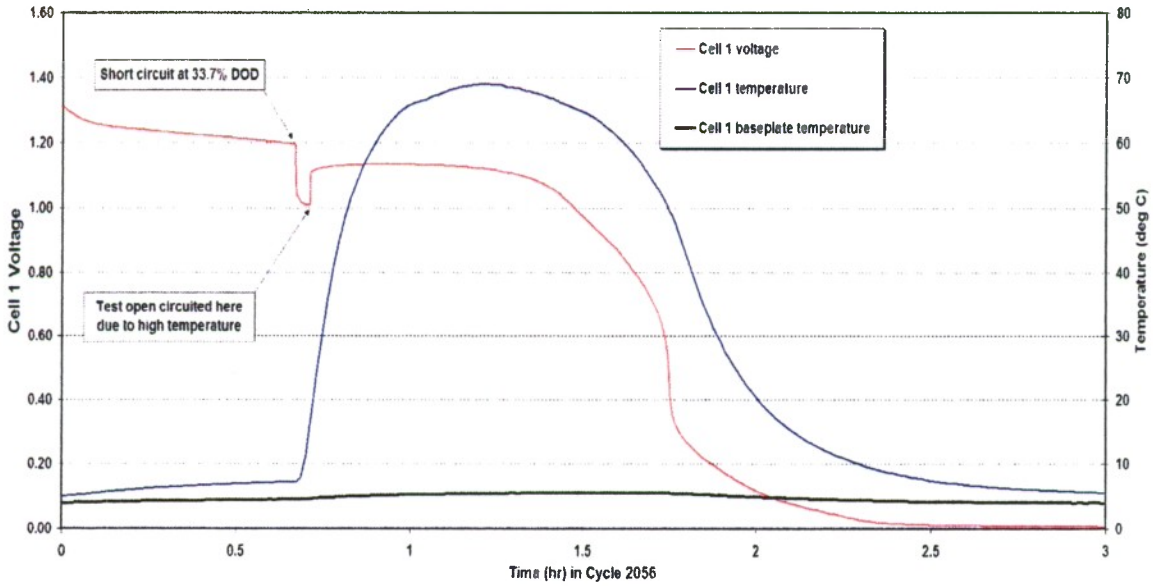

Figure 12. Voltage and thermal signatures during the failure of cell 1 at cycle 2056.

Disassembly of cell 1 showed that the hard short occurred when the core assembly on which the stack was mounted and constrained broke. The core assembly broke as the result of the core nut flying off the end of the threaded core. Upon removal of the stack compression, the stack expanded significantly on the side opposite the tabs on the nickel plates, while expanding much less on the side having the nickel plate tabs. The short circuit was on the side having the nickel plate tabs, and was a sufficiently hard short that it prevented the stack from being readily disassembled.

The root cause for the failure of cell 1 is clearly associated with significant expansion of the nickel electrodes as the result of nickel corrosion and cycling stresses in the 38% KOH electrolyte. The higher KOH concentration is known to contribute significantly to plate expansion caused by cycling, and the high pressure indicates significant corrosion of the sinter, which had 84% porosity at beginning of life. The expansion increased the compressive force on the core assembly until eventually it exceeded the force required to break the core assembly. Based on these results, in the future, it would not be surprising to see similar types of failures in cells 6 and 7, which also contain the higher electrolyte concentration.

7. Conclusions

Fourteen years of ground storage, followed by six years (2056 cycles) of life testing, have been completed on a matrix of nickel-hydrogen cell designs that was originally manufactured in 1988 to allow selection of an optimized ManTech cell design. Two of the eight cells on test have failed, and two other cells show signs of degradation due to separator dry out. These four cells that have either failed or degraded comprise all the cells in the test matrix that contained 38% KOH electrolyte. The cells containing 31% KOH electrolyte, which was the concentration selected in the optimized ManTech design that has been used widely in space applications, all continue to perform nominally. Thus, the results from this test to date validate the ManTech design that was selected and has been widely used over the last two decades, as the most robust design included in this test matrix.

After more than 2000 cycles, a novel voltage signature has been seen in the data from all four of the (originally) nickel-precharged cells in the test matrix. This may be significant because nickel precharge was selected over hydrogen precharge in the ManTech design due to its improved capacity stability during storage. This novel signature involves the emergence of a slightly depressed additional discharge voltage plateau between 1.1 and 1.2 V, which only emerged for the four cells originally having nickel precharge. This signature may arise from platinum-containing complexes that can form in the nickel electrode, and which have been reported in the literature to have a discharge plateau between 1.1 and 1.2 V. Interestingly, this slightly depressed secondary discharge plateau does not seem to correlate with cell capacity or performance degradation at this point in the life of these cells. Continued life testing, followed by analysis of electrodes from these cells, is expected to enable identification of the root cause for this novel voltage signature.

PHYSICAL SCIENCES LABORATORIES

The Aerospace Corporation functions as an "architect-engineer" for national security programs, specializing in advanced military space systems. The Corporation's Physical Sciences Laboratories support the effective and timely development and operation of national security systems through scientific research and the application of advanced technology. Vital to the success of the Corporation is the technical staff's wide-ranging expertise and its ability to stay abreast of new technological developments and program support issues associated with rapidly evolving space systems. Contributing capabilities are provided by these individual organizations:

Electronics and Photonics Laboratory: Microelectronics, VLSI reliability, failure analysis, solid-state device physics, compound semiconductors, radiation effects, infrared and CCD detector devices, data storage and display technologies; lasers and electro-optics, solid-state laser design, micro-optics, optical communications, and fiber-optic sensors; atomic frequency standards, applied laser spectroscopy, laser chemistry, atmospheric propagation and beam control, LIDAR/LADAR remote sensing; solar cell and array testing and evaluation, battery electrochemistry, battery testing and evaluation.

Space Materials Laboratory: Evaluation and characterizations of new materials and processing techniques: metals, alloys, ceramics, polymers, thin films, and composites; development of advanced deposition processes; nondestructive evaluation, component failure analysis and reliability; structural mechanics, fracture mechanics, and stress corrosion; analysis and evaluation of materials at cryogenic and elevated temperatures; launch vehicle fluid mechanics, heat transfer and flight dynamics; aerothermodynamics; chemical and electric propulsion; environmental chemistry; combustion processes; space environment effects on materials, hardening and vulnerability assessment; contamination, thermal and structural control; lubrication and surface phenomena. Microelectromechanical systems (MEMS) for space applications; laser micromachining; laser-surface physical and chemical interactions; micropropulsion; micro- and nanosatellite mission analysis; intelligent microinstruments for monitoring space and launch system environments.

Space Science Applications Laboratory: Magnetospheric, auroral and cosmic-ray physics, wave-particle interactions, magnetospheric plasma waves; atmospheric and ionospheric physics, density and composition of the upper atmosphere, remote sensing using atmospheric radiation; solar physics, infrared astronomy, infrared signature analysis; infrared surveillance, imaging and remote sensing; multispectral and hyperspectral sensor development; data analysis and algorithm development; applications of multispectral and hyperspectral imagery to defense, civil space, commercial, and environmental missions; effects of solar activity, magnetic storms and nuclear explosions on the Earth's atmosphere, ionosphere and magnetosphere; effects of electromagnetic and particulate radiations on space systems; space instrumentation, design, fabrication and test; environmental chemistry, trace detection; atmospheric chemical reactions, atmospheric optics, light scattering, state-specific chemical reactions, and radiative signatures of missile plumes.